## A novel whole-brain DTI segmentation technique for brain tumour delineation and diagnosis

Timothy L Jones<sup>1</sup>, B Anthony Bell<sup>1</sup>, and Thomas R Barrick<sup>2</sup>

<sup>1</sup>Academic Neurosurgery Unit, St Georges University of London, London, United Kingdom, <sup>2</sup>Stroke and Dementia Research Centre, St Georges University of London, London, United Kingdom

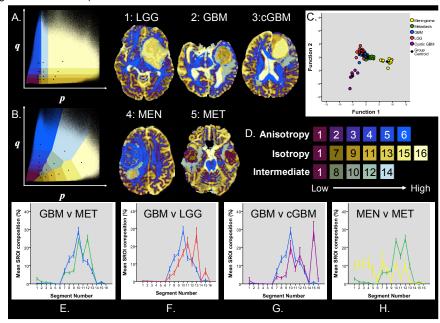
**INTRODUCTION:** Conventional MRI sequences have limited sensitivity and specificity in diagnosing brain tumours. Extent of contrast enhancement does not correspond with the boundary of tumour cellularity<sup>1,2</sup> which is critical when guiding maximal tumour resection and optimal radiotherapy target volumes. Previous studies have identified differences in diffusion patterns between tumour types<sup>3-5</sup> however this has yet to be applied in clinical practice. We present a novel whole brain DTI *k*-means clustering algorithm that generates tumour diffusion maps. When this technique is applied to cases of intracranial mass lesions, resultant maps display distinctive patterns for each tumour type with visually delineated boundaries.

**METHODS:** MRI scans were acquired from 94 patients with suspected intracranial mass lesions: 11 meningioma (MEN), 26 metastases (MET), 31 spin-echo planar images (b=1000 s mm<sup>-2</sup>) were acquired from 43 subjects using a 1.5T GE Signa LX (12 diffusion sensitised directions repeated 4 times) and 51 using a 1.5T GE Signa HD (61 diffusion gradient directions).

**DTI segmentation technique:** Histograms of p and q were computed across all brain voxels in all subjects simultaneously. High intensity noise was removed from the p and q distributions and all voxels above this threshold assigned to 1 and the remaining voxels scaled between 0 and 1. Initial cluster centroids were defined by separating p:q space into equal quartiles (lower quartile, median and upper quartile, fig. 1A). Using a k-means clustering algorithm, each image voxel,  $i \in I$ , was iteratively reclassified to one of 16 clusters based on the distance in (p,q) space of the voxel  $(p_0,q_i)$  to its nearest cluster median  $(m_p,m_q)$  by,

$$\min_{j \in \{1, \dots, 16\}} \sqrt{(p_i - m_{pj})^2 + (q_i - m_{qj})^2}$$

This was repeated for 250 iterations with steady state of classification reached before termination (fig. 1B). k=16 was selected *a priori* to identify potential tissue classes present within the tumour-affected brain. Including normal-appearing grey matter (NAGM), normal-appearing white matter (NAWM), cerebrospinal fluid (CSF), tumour mass (solid cellular component, necrosis, cyst and infiltrating margin), infiltrative peri-tumoural oedema and vasogenic oedema distant from the tumour.



**Visualisation technique:**  $T_2$ -weighted (b=0 s mm<sup>-2</sup>) images were scaled between 0 and 1 on a subject-by-subject basis. Median values for each of the 16 cluster centroids for p, q and  $T_2$ -value across the patient cohort were ranked (1 to 16). Rank scores were then assigned to the red channel ( $T_2$ -value), green channel ( $T_2$ ) and blue channel ( $T_2$ ) using a 24 bit RGB colour scheme. As the colour scheme is based on the ranks of the cluster centroids it is not affected by differences in magnitude between  $T_2$ ,  $T_2$  and  $T_2$ -weighted greyscale values. The colour key in fig 1D relates segment numbers to colours and cluster centroid ( $T_2$ ) properties.

Segmented region of interest (ROI) delineation: Tumour regions were semi-automatically delineated from the segmented colour maps using a 4-voxel neighbourhood recursive flood-filling algorithm. This was performed on all axial slices containing tumour or oedema to generate a 3D tumour ROI. The percentage contribution of each segment within this tumour region was calculated. The mean percentage contribution of each segment was calculated for each tumour type. This was plotted graphically to generate tumour 'spectra' (fig 1 E-H). A linear discriminant analysis (LDA) was performed to investigate which linear combinations of percentage contribution of each segment best discriminated between tumour types (fig 1C, colour key is shared with spectral graphs).

**RESULTS:** The technique generated colour maps with visually segmented boundary between tumour and normal brain with consistent colours for NAWM, NAGM and CSF spaces across subjects as well as tumour-specific colours. Example images are shown for each tumour type in fig 1 (LGG=1, GBM=2, cGBM=3, metastasis=4, meningioma=5). Spectral graphs allow comparison between tumour types (fig 1E-H). The salient results are as follows:

- Fig. 1E reveals increased cluster 12 in metastasis and increased cluster 8 in GBM. From the final Voronoi plot (fig 1B) and example images (fig 1: GBM and MET), it is evident this likely reflects different oedema characteristics between the tumours ('vasogenic' fluid-rich oedema in metastasis vs. 'infiltrative' cellular oedema in GBM).
- Greater proportion of clusters 7, 8, 9 and 10 are evident in GBM than LGG, which has increased proportion of cluster 13, fig.1F. This reflects greater tumour cell density in malignant gliomas (therefore lower isotropy than the diffuse cellularity in LGG).
- cGBM exhibit increased cluster 14 (fig. 1G) due to their constituent fluid compartment.
- Meningiomas have greater proportion of clusters1-5 due to their densely packed, highly organised cellular microstructure (fig 1H).

The LDA (fig 1C) correctly classifies tumour type in 83 out of 94 cases (cross-validated *post hoc*), yielding diagnostic sensitivities of 83.9% GBM, 100% cGBM, 84.2% LGG, 72.7% meningioma and 92% metastasis with corresponding specificities of 95.5, 100, 94.9, 100 & 91.9%, respectively.

**DISCUSSION:** This is one of the largest studies to date of diffusion tensor imaging in brain tumour diagnosis. Our segmentation technique reveals improved diagnostic sensitivities and specificities than previously reported manual DTI-ROI drawing techniques<sup>6</sup> for a greater range of tumour types. Combining clustered images with their corresponding Voronoi plot of *p:q* space allows interpretation of regional diffusion characteristics and thus potentially tissue structure. Automatic tumour region of interesting techniques offer a fast, reproducible method of tumour diagnosis and may have a further role in delineating tumour regions for surgery and radiotherapy planning as well as the longitudinal surveillance of tumours pre or post treatment

- (1) Burger PC, et al J Neurosurg 1988; 68(5):698-704.
- (2) Watanabe M et al Neuroradiology 1992; 34(6):463-469.
- (3) Lu S et al Radiology 2004; 232(1):221-228.
- (4) Pierpaoli et al **Radiology** 1996; 201(3):637-648.
- (5) Provenzale et al Radiology 2004; 232(2):451-460.
- (6) Wang S et al Neuroimage 2009; 44(3):653-660.